

# Journal of Advanced Research Design



Journal homepage: https://akademiabaru.com/submit/index.php/ard ISSN: 2289-7984

# Enhancing Medical Image Quality with Efficient Denoising Techniques Using Hybrid Methods

Noor Huda Ja'afar<sup>1,\*</sup>, Sairul Izwan Safie<sup>1</sup>, Afandi Ahmad<sup>2</sup>, Zarina Tukiran<sup>2</sup>

- Section of Instrumentation and Control Engineering, Universiti Kuala Lumpur Malaysian Institute of Industrial Technology, Persiaran Sinaran Ilmu, Bandar Seri Alam, 81750 Masai, Johor, Malaysia
- Department of Eletronic Engineering, Faculty of Electrical and Electronic Engineering, Universiti Tun Hussein Onn Malaysia, Persiaran Tun Dr. Ismail, 86400 Parit Raja, Johor, Malaysia

#### **ARTICLE INFO**

#### **ABSTRACT**

#### Article history:

Received 23 June 2025 Received in revised form 26 July 2025 Accepted 14 August 2025 Available online 1 November 2025 New technologies in the healthcare industry are revolutionizing the use of medical modalities, from simple measurement devices to complex systems like Computed Tomography (CT) scanners, Magnetic Resonance Imaging (MRI), Positron Emission Tomography (PET), and Ultrasound machines. However, the medical imaging acquisition process and subsequent processing stages can introduce noise and artifacts, which can adversely affect the accuracy of medical diagnoses and treatments. This paper presents the development of an enhanced denoising technique using a hybrid method that combines Fast Discrete Wavelet Transform (FDWT) and Fast Discrete Curvelet Transform (FDCvT) algorithms. The limitations of wavelets in handling curves and edges are mitigated by the curvelet transform, thereby directly improving imaging performance. Three different approaches, based on various wavelet families, are proposed: Daubechies (Approach-1), Coiflet (Approach-2), and Biorthogonal (Approach-3) wavelet transforms. To create a robust denoising system, Gaussian noise is added to the original images. The noisy images are first decomposed into several sub-bands using the FDWT algorithm. The wavelet coefficients generated are then separated into different orientations using the wrapping-based FDCvT algorithm. These wavelet coefficients are wrapped around a periodic extension of themselves. By effectively addressing the limitations of wavelets in handling curves and edges, the hybrid method enhances imaging performance across various medical modalities, including MRI, CT, and PET. The evaluation using Peak Signal-to-Noise Ratio (PSNR) and Structural Similarity Index (SSIM) confirms that the proposed approaches significantly outperform existing benchmark techniques. Specifically, Approach-2 shows a 25 % reduction in noise for CT images, while Approach-3 yields a substantial 15 % improvement in Gaussian denoising. These findings highlight the potential of the hybrid method to improve the accuracy and reliability of medical diagnoses and treatments by reducing noise and artifacts in medical images.

#### Keywords:

Medical image; denoising; wavelet; curvelet

\* Corresponding Author.

E-mail address: noorhuda.jaafar@unikl.edu.my

#### 1. Introduction

In today's ever-evolving healthcare landscape, the integration of advanced technologies is reshaping the utilization of medical modalities. From fundamental medical measurement instruments such as body temperature gauges, electrocardiographs, blood sugar level monitors, and blood pressure monitors to sophisticated machinery like Computed Tomography (CT) scanners, Magnetic Resonance Imaging (MRI) equipment, Positron Emission Tomography (PET) scanners, ultrasound devices, and X-ray machines, the substantial influence of cutting-edge technology is evident across the industry [1]. According to National Health Services (NHS) statistics, an enormous number of medical images are generated each year [2]. The generation of medical images for various modalities has increased from 2012 to 2021. Medical image data is amassing at an alarming rate and is presently overwhelming. Additionally, since the use of medical images in telemedicine applications has expanded, there is a greater need in the medical professions for fast and efficient coding algorithms [3]. In its broadest sense, telemedicine is the practice of providing medical treatment remotely while facilitating contact between patients and medical professionals. It overcomes geographic restrictions and enhances accessibility to healthcare by enabling healthcare professionals to diagnose, treat and monitor patients at a distance.

In general, different medical imaging technologies generate images using various analogies. The electromagnetic energy spectrum serves as the primary energy source for images at the moment [4]. One of the medical imaging modalities used in radiology to observe intricate internal structures is MRI or Nuclear Magnetic Resonance (NMR) [3]. Radio waves are used in MRI, which involves passing brief radio wave pulses through a patient. Each of these pulses is followed by a return pulse of radio waves produced by every tissue. Also, MRI has benefits for visceral imaging, such as cancer detection and the imaging of the brain, muscles, heart, and other organs [6]. On the other side, a PET scan is an effective way to help identify a variety of conditions, including cancer, heart disease and brain disorders. It makes use of the interaction between gamma rays with the biologically active molecule in the human body to generate a 2-D image. Also known as X-ray computed tomography, CT is one of the medical imaging techniques that use multiple X-rays (ionizing radiation) to create a slice image of the human body. All the medical imaging modalities mentioned, notably share common properties to generate the slices of image and are used as the test image in this research.

As illustrated in Figure 1, the two-dimensional (2-D) data set is represented by a group of 2-D slice images like slices in a loaf of bread [7]. Commonly, human body tissues will be integrated together to build the 2-D models when the source and detector rotate continuously around the patients. After that, the results of the 2-D image are visualized into the visualization workstation such as a computer. From there, the 2-D image is analyzed in detail to detect any changes from the normal 2-D image visualization. On top of that, noise and artefacts may be added to the images as a consequence of the acquisition processes for medical imaging. Therefore, it is more challenging for medical experts in interpreting the images due to the effects of the added noise. Indirectly, it may have a negative impact on the accuracy of medical diagnosis and treatment.

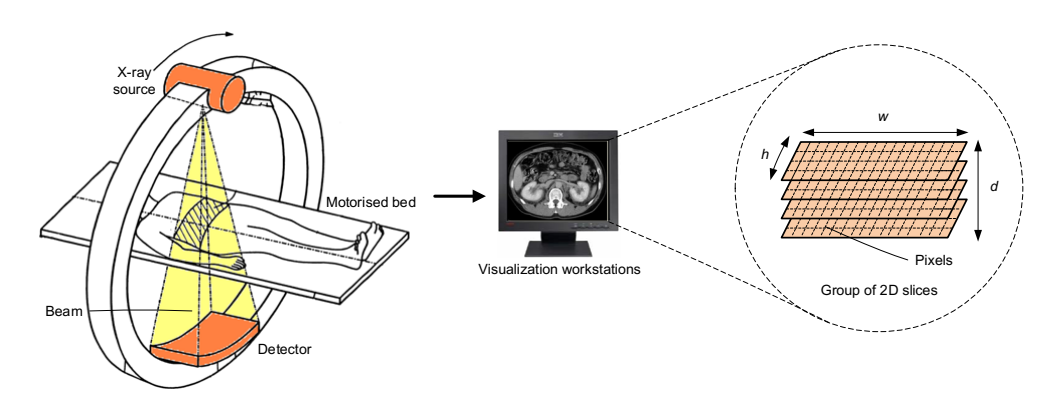


Fig. 1. Medical image data processing

Generally, noise is introduced into an image during image transmission, acquisition, coding or processing procedures [8]. It is a random variation of brightness or color information in images and an undesirable by product of the image that obscures the desired information. Hence, image denoising plays an important role in a wide range of applications such as image restoration, visual tracking, image registration, image segmentation, image compression and image classification, where obtaining the original image content is crucial for strong performance [9]. While many algorithms have been proposed for the purpose of image denoising, the problem of image noise suppression remains an open challenge, especially in situations where the images are acquired under poor conditions where the noise level is very high. Furthermore, real-time medical image processing applications also utilize several fundamental operations like matrix and vector applications in their algorithms. The majority of these operations include matrix transformations, such as the Discrete Cosine Transform (DCT), Fast Fourier Transform (FFT), Discrete Wavelet Transform (DWT) and other recently created transforms as the finite Radon, Curvelet, and Ridgelet transform [10]-[13].

The contribution of this paper is described as follows: (1) Developing the denoising technique using a hybrid method; the combination of the Fast Discrete Wavelet Transform (FDWT) and Fast Discrete Curvelet Transform (FDCvT). (2) Analyzing the performance of the denoising techniques using different approaches; Approach-1 uses the Daubechies, Approach-2 applies Coiflet and Approach-3 uses Biorthogonal wavelet transforms with two objective evaluations; Peak Signal-to-Noise Ratio (PSNR) and Structural Similarity Index (SSIM).

#### 2. Related Works

Medical images often contain signal-dependent noise, which is a type of noise that varies with the signal intensity [14]. The signal-dependent noise is correlated with the image intensity, making it difficult to distinguish it from the actual image features. Additionally, different medical imaging modalities are susceptible to different types of noise and understanding the sources and effects of these noises is important for accurate image interpretation and diagnosis. In many medical imaging systems, medical image denoising is an essential pre-processing step because of the current issues. Denoising an image can generally be done in a number of ways, including wavelet-based filtering, deep learning-based algorithms, and spatial filtering [15–18]. The value of a pixel is substituted with the median value of the pixels in its surrounding neighborhood in spatial filtering techniques like median filtering. Contrarily, wavelet-based filtering divides an image into several frequency subbands and then applies denoising to each sub-band using wavelet transforms. Convolutional Neural

Networks (CNNs), for example, use deep learning to learn the procedure for denoise an image by training on a huge dataset of both noisy and original images. The techniques for medical image denoising from the previous works are reviewed in the paragraphs that follow.

An implementation of contourlet transform using adaptive threshold for medical image denoising system is proposed in [19]. In this study, an algorithm to define a new threshold value to eliminate the corrupted pixels or noise is concerned. Initially, the contourlet transform is applied to the noisy image and produces the contourlet coefficients. The threshold value is used as a criterion to identify which coefficients are significant and which ones are less important. If the coefficients are greater than the threshold, those coefficients are considered important and are left unchanged. Otherwise, those coefficients are considered less important and are suppressed. Finally, the inverse contourlet transform is applied to reconstruct the denoising image. Experimentally, better performance in terms of Mean Squared Error (MSE) and PSNR is achieved compared to the wavelet transform method. However, the researchers only use one type of medical imaging, which is an MRI image, to evaluate the proposed technique.

Jameel [20] have propose a new image denoising method using combination of Wavelet Transform (WT) and Multi-Wavelet Transform (MWT). Both WT and MWT are cascaded to increase the denoising performance. Theoretically, a WT computation is based on single scaling function and mother wavelet and the decomposition generates four sub-bands; low-low (LL), low-high (LH), high-low (HL) and high-high (HH). In contrast, MWT uses several scaling functions and mother wavelets to break down the coefficients. The MRI image is initially corrupted by Gaussian noise. Then, the MWT is applied to the noisy image and generates four sub-bands, where the first sub-band is the approximated information of the noisy image and another three sub-bands are the details of the background of the noisy image. The success of implementing the proposed method was hypothetically proved based on the simulation results, where the denoising performance in terms of PSNR value is improved.

Another issue on the medical image denoising is presented in [21]. A denoising of the medical image using deep CNN model is proposed. The proposed model uses a combination of deep residual layers with Batch Normalization (BN) to achieve stability and precipitate the training process. In deep learning, each layer in the network is trained to extract meaningful features from the input data. The proposed CNN-based model consists of three layers, which are feature extraction, feature conversion and residual image generation. Referring to the training process, 64 filters with size 4×3×3 are utilized in the feature extraction layer. Whilst, a single filter of size 64×3×3 is applied in the residual image generation layer to regenerate the denoised image. Multiple medical imaging such as US, MRI, CT and MRI are used to evaluate the proposed method. The simulation results show that the proposed CNN model dealing with CT and MRI images provides efficient performances compared to other denoising techniques. Regardless of the better performance obtained, the combination of the CNN with other transforms is expected to obtain better results.

Aslam et al. [22] have proposed a new technique for the removal of noise using hybrid filters. In general, a hybrid filter is a combination of two or more filters that aims to achieve improved performance. Thus, in this study, the combination of a modified median filter and wiener filter is used to provide improved results in terms of removing noise from signals, while preserving their important features. The median filter was modified by taking the median value to determine the new median value. This technique conserves the edges and makes them more stable, but, the details of the modified median filter are not discussed in this paper. The original RGB MRI image is first converted into a grayscale image. Then, some Gaussian noise is added along with mean and variance values. To make the original image more visible, the modified median filter is then applied to the noisy image. The wiener filter is continuously modified to eliminate all noise. Even though the experiment results

exhibit a high PSNR value, no comparison results are conducted with the previous or existing techniques.

A novel medical image denoising method based on Conditional Generative Adversarial Network (CGAN) is proposed in [23]. The main objective of this paper is to investigate the viability of the CGAN method for medical image denoising by applying different types of noise. Basically, Generative Adversarial Network (GAN) is a deep learning framework designed for generating new data samples from a given distribution. The basic GAN is composed of two neural networks, which are a Generator (G) network and a Discriminator (D) network. The generator tries to produce samples that the discriminator cannot distinguish from real samples, while the discriminator tries to correctly identify which samples are real and which are fake. With the addition of Gaussian and salt and paper noise to the X-ray and CT images, the results exhibit that applying the CGAN module enhances the quality of the denoised images. However, implementing the several layers and RDBs in the proposed framework touches on the algorithm's complexity.

Another medical image denoising method is proposed by Thamilselvan in [24]. The proposed method uses a Pre-processing Profuse Clustering Technique (PPCT) algorithm. Generally, the pre-processing step is an important one in clustering, as it can significantly impact the quality of the results. An effective pre-processing step can result in improved clustering results and more meaningful insights. The PPCT algorithm consists of five steps, starting with the Simple Linear Iteration Clustering (SLIC) calculation until reconstructing the denoised image. Various denoising techniques are taken into count in comparing the performance of the proposed method, such as Non-Nearby Means (NLM), K-means-Singular Vector Decomposition (K-SVD), Block Matching and 3-D filtering (BM3D). The results exhibit that the pre-processing steps have an impact on the performance of the proposed method.

All the previous works discussed are summarized in Table 1. The summarization is based on the types of medical images, the denoising method, the addition noise used and the performance evaluation parameters. The most often used approaches for denoising are those that rely on deep learning and transforms. On the other hand, Gaussian noise is completely utilized in the earlier works, supporting its suitability for use in image tampering. Additionally, the input medical images used to experimentally analyze the performance are another topic of concern. Solely the works in [21] and [23] used more than one medical image; all other works solely used MRI images. If different input data are taken into account when evaluating the performance, efficient findings might theoretically be obtained. In terms of performance evaluations, the MSE and PSNR values are widely used in performance evaluations and is an important metrics to compute. Calculating the Structural Similarity Index (SSIM) value is necessary to assess the denoised image's quality.

**Table 1**Summary of the previous works

	Medical image	Methods	Noise	Performance evaluations		
Refs.			-	MSE	PSNR	CPU time (s)
[19]	MRI	Contourlet Transform	Gaussian	<b>√</b>	✓	
[20]	MRI	MWT and WT	Gaussian	$\checkmark$	$\checkmark$	
[21]	Ultrasound, X-ray, CT, PET, MRI	CNN	Gasussian	✓	✓	✓
[22]	MRI	Modified median and weiner filter	Gaussian	✓	✓	
[23]	X-ray, CT	CGAN	Gaussian, salt and pepper	✓	✓	
[24]	MRI	PPCT	Gaussian	$\checkmark$	$\checkmark$	

### 3. Mathematical Algorithms

This section presents the FDWT algorithm, specifically using Daubechies, Coiflet, and Biorthogonal wavelet transforms. Additionally, it elaborates on a wrapping-based method for FDCvT algorithms.

# 3.1 Fast Discrete Wavelet Transform (FDWT)

Bigger tile sizes can prevent blocking artefacts when using the FDWT technique, which uses a frame-based processing paradigm. The image can be divided into numerous tiles using this method. A low-pass and a high-pass filter are the two filters that make up the FDWT processes. The outputs from the high-pass and low-pass filters, respectively, provide the detail coefficients and approximation coefficients. Interestingly, the wavelet transform is superior to multiresolution analysis; the approximation coefficients can be fed into another pair of low-pass and high-pass filters. According to Nyquist's rule, the bandwidth of the signal being sampled must be less than half of the frequency of the sampling clock. Hence, the outputs of both low-pass and high-pass filters are down sampling by factor of two to reduce the data rate of the signal. Figure 2 shows the block diagram of filter bank analysis for FDWT with two level decompositions. The alphabet *L* represents the approximated signal whilst alphabet *H* represent the detail signal.

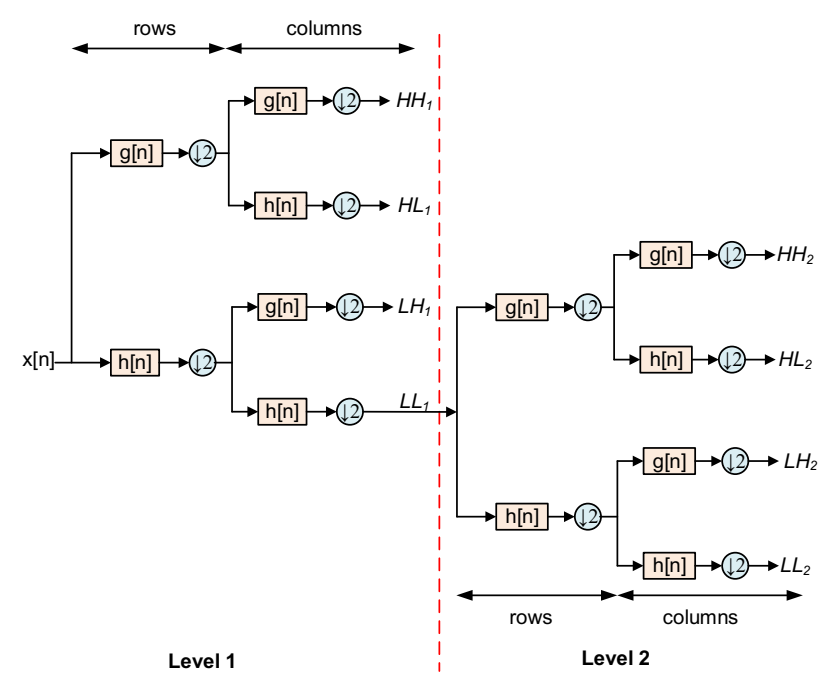


Fig. 2. A filter analysis for two-level FDWT decomposition

Three types of wavelet filters are used in the proposed approaches; Daubechies (Db), Coiflet (Coif) and Biorthogonal (Bior), represented by Approach-1, Approach-2 and Approach-3, respectively. Each wavelet transform has a unique algorithm that uses scaling and wavelet functions. The Db and Coif wavelets have basic symmetric functions, while the Bior wavelet has asymmetric basic functions. The scaling and wavelet functions for Db, Coif and Bior wavelet transforms are given in Table 2. Theoretically, a wavelet with more vanishing moments can more accurately represent a broader range of functions. Thus, this research work considers a higher number of wavelet families.

**Table 2**The scaling and wavelet functions for Db, Coif and Bior wavelet transforms

Wavelet types	Scaling function	Wavelet function
Db	$\phi(x) = \sum h(n)\phi(2x - n)$	$\psi(x) = \sum g(n)\phi(2x-n)$
Coif	$\phi(x) = \sum h(n)\phi(2x - n)$	$\psi(x) = \sum g(n)\phi(2x-n)$
Bior	$\phi(x) = \left(1 + \sqrt{3}\right) / \left(4\sqrt{2}\right) *$	$\psi(x) = \left(1 - \sqrt{3}\right) / \left(4\sqrt{2}\right) *$ $\left(S(x) - S(x-1) + \sqrt{3S(x-2)}\right)$
	$\left(\delta(x)+\delta(x-1)+\sqrt{3\delta(x-2)}\right)$	$\left(\delta(x)-\delta(x-1)+\sqrt{3}\delta(x-2)\right)$

# 3.2 Fast Discrete Curvelet Transform (FDCvT)

A second generation of the curvelet transform, called FDCvT is a high-dimensional wavelet transform used to analyze an image with different scales and directions. It is designed for handling curves and other singularities in medical images. The multiresolution architecture of curvelet transform provides a new dimension to the multidimensional theory. The transform maps an image into a set of curvelets, which are complex functions that capture the directional and scale information of image features. Another advantage offered by curvelet transform is a multiscale analysis. Curvelet is said to be a parabolic scaling relation in space with a condition width≈length² when a curvelet at

scale is oriented "needle" and effectively support  $2^{-j}$  by  $2^{-j/2}$  a rectangle. On the other side, a curvelet at scale is a "wedge" whose frequency support is inside a rectangle with size  $2^j$  by  $2^{j/2}$ . The curvelet transform is defined as the inner product of the function f to be analyzed and a family of curvelets  $\gamma_{ab\theta}$  as recorded in Eq. (1).

$$\Gamma_f(a,b,\theta) = \langle f, \gamma_{ab\theta} \rangle \tag{1}$$

where a>0 is the scale parameter, b is the translation parameter and  $\emptyset \in [0,2\pi)$  is the orientation parameter. The symbol  $\Gamma_f$  represents the curvelet transform. The family of curvelets is explained by starting with two smooth, non-negative, real-valued windowing functions called the radial window W(r) and the angular window V(t), respectively. The discrete curvelet transform is often used to process the function f, which also starts with two window functions: the radial window W(r) and the angular window V(t).

Generally, there are two major revisions of the curvelet transform, called the first and second generations of the curvelet transform. The first generation also known as curvelet-99, uses complex procedures, including ridgelet analysis. To overcome the drawback of the first generation, the ridgelet analysis is skipped in the second generation of the curvelet transform and known as the FDCvT. In addition, the curvelet coefficients can be determined using the wrapping-based method or the unequally spaced fast Fourier transform (USSFT) process. The wrapping-based method makes computation time faster and more efficient compared to the USSFT method. Therefore, in this work, the wrapping-based method has been selected. Figure 3 depicts a polar frequency plane with radial windows in discrete coronae for supporting curvelets of a scale in different orientations. The shaded area illustrates a narrow radial wedge centered at a long radial frequency line but with a short width in angular frequency compliant with the parabolic scaling rule. It provides the frequency support of the curvelet centered in a specific spatial orientation,  $\emptyset_1$ .

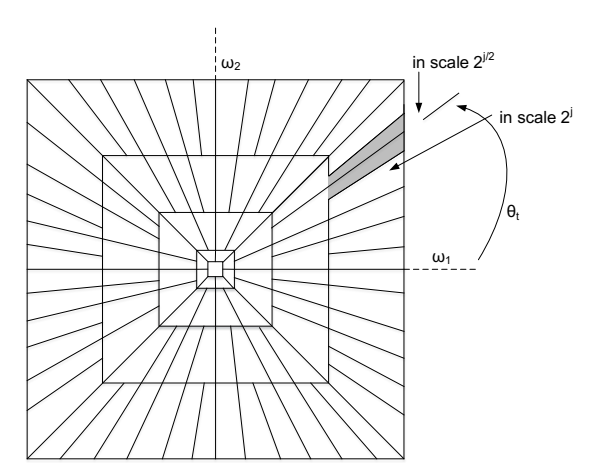


Fig. 3. The 2-D discrete curvelet transform frequency plane

### 4. Proposed Method: Denoising Technique using Hybrid Method

In this section, a combination of FDWT and FDCvT wrapping-based algorithms is employed. As shown in Figure 4, the proposed denoising technique involves five stages: image corruption, FDWT decomposition, FDCvT decomposition, thresholding, and reconstruction. The novel aspects of the approach are in stages two and three, focusing on decomposition using the hybrid transform-based technique. There are three approaches, highlighted in blue: Approach-1 uses Daubechies-12 (Db12),

Approach-2 applies Coiflet-6 (Coif6), and Approach-3 uses Biorthogonal-6.8 (Bior6.8) wavelet transforms.

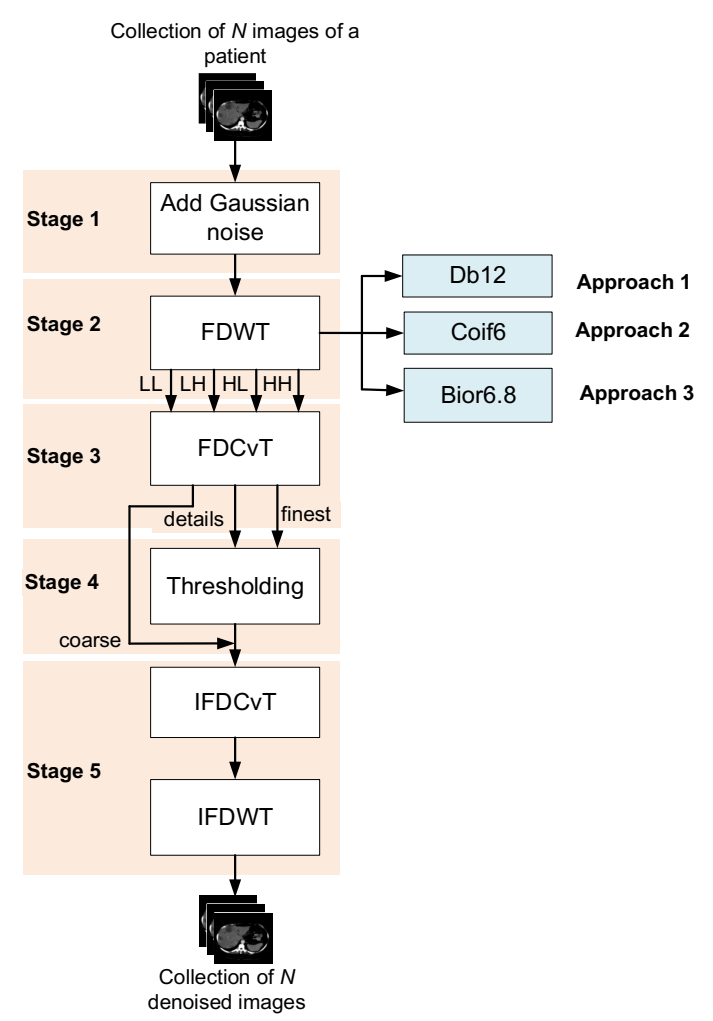


Fig. 4. The block diagram of the proposed denoising technique

#### 4.1 Stage 1: Image Corruption

The original image in this proposed work has been corrupted using Gaussian noise; a statistical noise with a normal distribution. The choice of Gaussian noise was made because it could be introduced to a variety of medical imaging. This indicates that the noise levels have a normal Gaussian distribution. Initially, the original image is supplemented with the Gaussian noise. Then, the probability density function,  $\rho$  of a Gaussian random variable, z is calculated using the formula shown in Eq. (2).

$$\rho_G(z) = \frac{1}{\sigma\sqrt{2\pi}}e^{-\frac{(z-\mu)^2}{2\sigma^2}} \tag{2}$$

where z represents the grey level,  $\mu$  is the mean value and  $\sigma$  is the standard deviation.

### 4.2 Stage 2: FDWT Decomposition

The noisy image's spatial domain is next converted to its frequency domain. Three different wavelet filter types are employed in the proposed approaches, as described in Section 4; these are

Db12, Coif6, and Bior6.8, which are represented by Approaches 1, 2 and 3, respectively. The wavelet coefficients for the Db12, Coif6 and Bior6.8 wavelet transforms are listed in Table 3.

**Table 3**The wavelet coefficients for Db12, Coif5 and Bior6.8

Approach	Wavelet family	Scaling coefficients, h(n)		Wavelet coefficients, $g(n)$	
Approach-1	Db12	h(0) = 0.1115 $h(1) = 0.4945$ $h(2) = 0.7511$ $h(3) = 0.3153$ $h(4) = -0.2263$ $h(5) = -0.1298$	h(6) = 0.0975 $h(7) = 0.0275$ $h(8) = -0.0316$ $h(9) = 0.0006$ $h(10) = 0.0048$ $h(11) = -0.0011$	g(0) = h(11) $g(1) = -h(10)$ $g(2) = h(9)$ $g(3) = -h(8)$ $g(4) = h(7)$ $g(5) = -h(6)$	g(6) = h(5) $g(7) = -h(4)$ $g(8) = h(3)$ $g(9) = -h(2)$ $g(10) = h(1)$ $g(11) = -h(0)$
Approach-2	Coif5	h(0) = 0.0386 $h(1) = -0.1270$ $h(2) = -0.0771$ $h(3) = 0.6075$ $h(4) = 0.7457$ $h(5) = 0.2266$	h(6) = -0.1298 $h(7) = -0.2498$ $h(8) = 0.0666$ $h(9) = 0.2742$ $h(10) = -0.1623$ $h(11) = -0.4120$	g(0) = h(11) $g(1) = -h(10)$ $g(2) = h(9)$ $g(3) = -h(8)$ $g(4) = h(7)$ $g(5) = -h(6)$	g(6) = h(5) $g(7) = -h(4)$ $g(8) = h(3)$ $g(9) = -h(2)$ $g(10) = h(1)$ $g(11) = -h(0)$
Approach-3	Bior6.8	h(0) = 0.0015 $h(1) = -0.0030$ $h(2) = -0.0129$ $h(3) = 0.02892$ $h(4) = 0.0530$ $h(5) = -0.1349$ $h(6) = -0.1638$ $h(7) = 0.4626$ $h(8) = 0.9516$	h(9) = 0.4626 $h(10) = -0.1638$ $h(11) = -0.1349$ $h(12) = 0.0530$ $h(13) = 0.0289$ $h(14) = -0.0129$ $h(15) = -0.0030$ $h(16) = 0.0015$	g(0) = -h(16) $g(1) = h(15)$ $g(2) = -h(14)$ $g(3) = h(13)$ $g(4) = -h(12)$ $g(5) = h(11)$ $g(6) = -h(10)$ $g(7) = h(9)$ $g(8) = -h(8)$	g(9) = h(7) $g(10) = -h(6)$ $g(11) = h(5)$ $g(12) = -h(4)$ $g(13) = h(3)$ $g(14) = -h(2)$ $g(15) = h(1)$ $g(16) = -h(0)$

# 4.3 Stage 3: FDCvT Decomposition

The wavelet coefficients generated from stage 2 are further processed using FDCvT wrapping-based method. The computation of the curvelet algorithm requires three primary parameters: the number of scales  $n_{\text{scales}}$ , the number of orientations  $l_j$  and the number of angular panels  $n_{\text{quad}}$ . In curvelet domain, the information of prominent edges or curved elements in images is packed into a small number of coefficients, thus the transform yields a very sparse image representation. Through the Plancherel's theorem, the curvelet coefficients are also given by the inner products in the frequency domain as written in Eq. (3).

$$c(j,l,k) = \langle f, \varphi_{j,\theta_{l},k} \rangle := \frac{1}{(2\pi)^{2}} \langle \hat{f}, \hat{\varphi}_{j,\theta_{l},k} \rangle = \frac{1}{(2\pi)^{2}} \int \hat{f}(\omega) \overline{\hat{\varphi}_{j,\theta_{l},k}(\omega)} d\omega$$

$$= \frac{1}{(2\pi)^{2}} \int \hat{f}(\omega_{l}, \omega_{2}) U_{j}(R_{\theta_{l}}\omega) e^{i(k_{l}\omega_{l}+k_{2}\omega_{2})} d\omega_{l} d\omega_{2}$$
(3)

The magnitude of curvelet coefficients c(j,l,k) denotes the strength of the curved singularity, a short edge segment at scale j centered at the location  $k=(k_1,k_2)$  and in orientation  $\emptyset_l$ . In digital implementation, the polar wedge is replaced by the pseudo polar wedge in the Cartesian coordinates as shown in Figure 5 (b). The mathematical operation of FDCvT via the wrapping-based method is referred to as follows:

- i. Implement the FFT algorithm to the image.
- ii. Partition the FFT coefficients into a group of digital tiles.
- iii. For each tile:
  - a. Simplify the tile to the origin.
  - b. Wrap the tile's parallelogram-shaped support around a rectangle centered at the origin.
  - c. Implement the inverse FFT algorithm to the wrapped support.

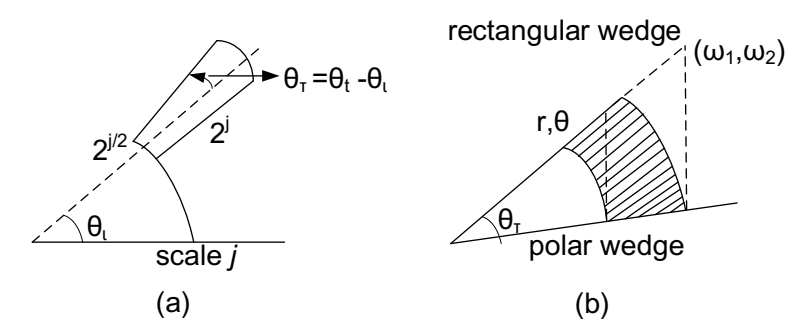


**Fig. 5.** A polar wedge constructed for scale j and orientation  $\theta_i$  (a) Frequency domain (b) Polar wedge

#### 4.4 Stage 4: Thresholding

A hard thresholding technique is used to threshold the details and the finest coefficients. The coarse coefficients, on the other hand, are not thresholded and are given directly to the subsequent stage. Eq. (4) depicts the formula to calculate the threshold value, where S is the number of levels starting with the second level and C is the curvelet coefficients. This algorithm removes all pixel or signal values below the threshold by applying the hard thresholding operator element-wise to the picture or signal. Only the signal or pixel values higher than the threshold are kept in the final denoised image or signal; these values are thought to represent the true signal or image content. The noise and signal properties are typically used to determine the threshold value, T. After the details and finest coefficients have been processed, both coefficients are combined with the coarse coefficients before being applied with the inverse transform-based method in the next stage.

$$T = 3*sigma + sigma*(s == length(C))$$
(4)

# 4.5 Stage 5: Reconstruction

This process is undertaken during the denoising of the image. It reverses each of the proposed decomposition stages to remodeling the original image. This stage consists of two transform-based algorithms; inverse FDCvT and inverse FDWT. In addition, three approaches are involved in the IFDWT algorithm, depending on the decomposition approach in stage 2. The general algorithm employed in the reconstruction stage is as follows:

Step 1: Read the threshold coefficients.

Step 2: Apply the inverse FDCvT algorithm.

Step 3: Apply the inverse FDWT algorithm.

Step 4: Display the denoised image.

#### 5. Results and Discussions

This section evaluates the effectiveness of the suggested robust and imperceptible denoising technique. Objective quantitative analysis is used to evaluate the proposed techniques. Numerous attacks with varying parameters were performed to access robustness further. Finally, the proposed technique's imperceptibility and robustness are compared to state-of-the-art works.

#### 5.1 Experiment Setup

The experiment used MATLAB R2022b with Windows 10 Pro (64-bit), Intel Core i5 processor 8 GB RAM. The proposed denoising techniques were executed using MATLAB live script to observe the simulation results. Moreover, this experiment uses the grayscale format and image size 512×512 of the medical image. A total of three medical images from different modality types were used as test data, including MRI, PET and CT images. The medical images were retrieved the Cancer Imaging Archive (TCIA), National Institutes of Health (NIH) [2].

# 5.2 Performance Evaluations

The performance of the proposed denoising techniques are measured using three (3) objective evaluations; MSE, PSNR and SSIM. The formula to calculate the MSE, PSNR and SSIM is given in Eq. (5), (6) and (7), respectively.

$$MSE = \frac{1}{n} \sum_{i=1}^{n} \left( Y_i - \hat{Y}_i \right)^2 \tag{5}$$

where n is the total number of pixels in the image,  $Y_i$  is the value of the i-th pixel in the original image and  $\hat{Y}_i$  is the value of the i-th pixel in the denoised image.

$$PSNR = 20\log 10(MAX_i) - 10\log 10(MSE)$$
(6)

where  $MAX_i$  is the maximum possible pixel value of the image (255 for 8-bits).

$$SSIM(x,y) = \frac{(2\mu_x \mu_y + c_1)(2\sigma_{xy} + c_2)}{(\mu_x^2 \mu_y^2 + c_1)(\sigma_x^2 \sigma_y^2 + c_2)}$$
(7)

where  $\mu_x$  is the pixel sample mean of x,  $\mu_y$  is the pixel sample mean of y,  $\sigma_x^2$  is the variance of x,  $\sigma_y^2$  is the variance of y,  $\sigma_{xy}$  is the covariance of x and y,  $c_1 = (k_1 L)^2$ ,  $c_2 = (k_2 L)^2$  are two (2) variables to stabilise the division with weak denominator, L is the dynamic range of the pixel-values,  $k_1 = 0.01$  and  $k_2 = 0.03$ .

#### 5.3 Results

Figures 6 to Figure 8 illustrate the results of the proposed denoising technique for different diagnoses cases using CT, MRI and PET images, respectively. The PSNR values for the noisy and denoised images are calculated to assess the level of distortion in the reconstructed images. Theoretically, a higher PSNR value indicates that the reconstructed image is closer in quality to the original image.

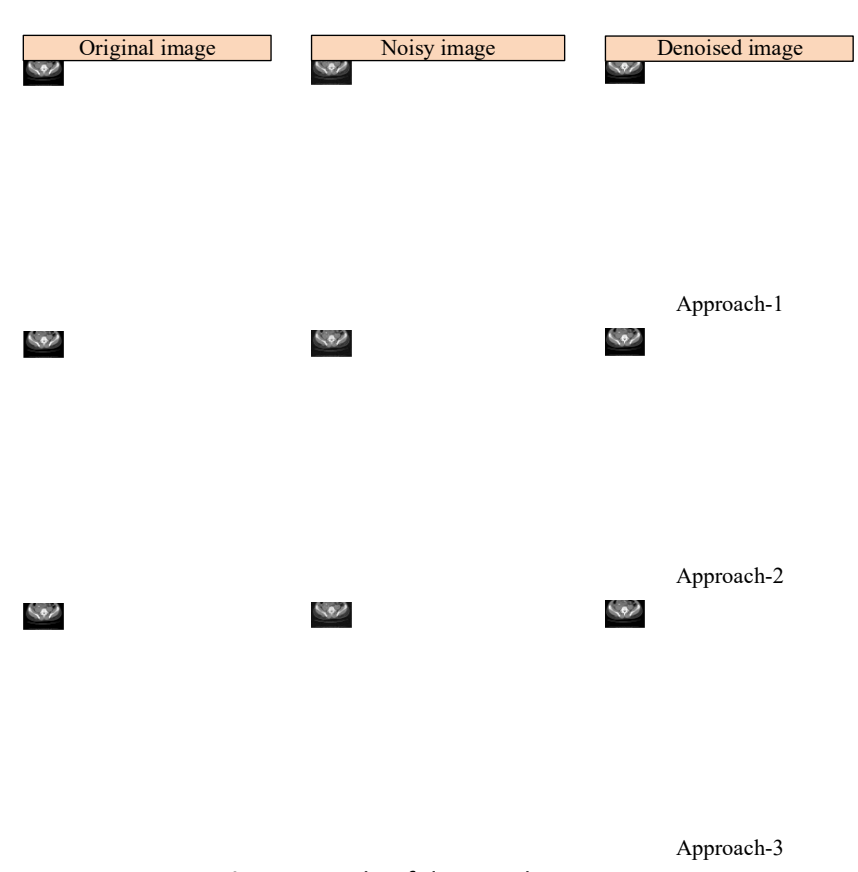


Fig. 6. Sample of denoised CT images

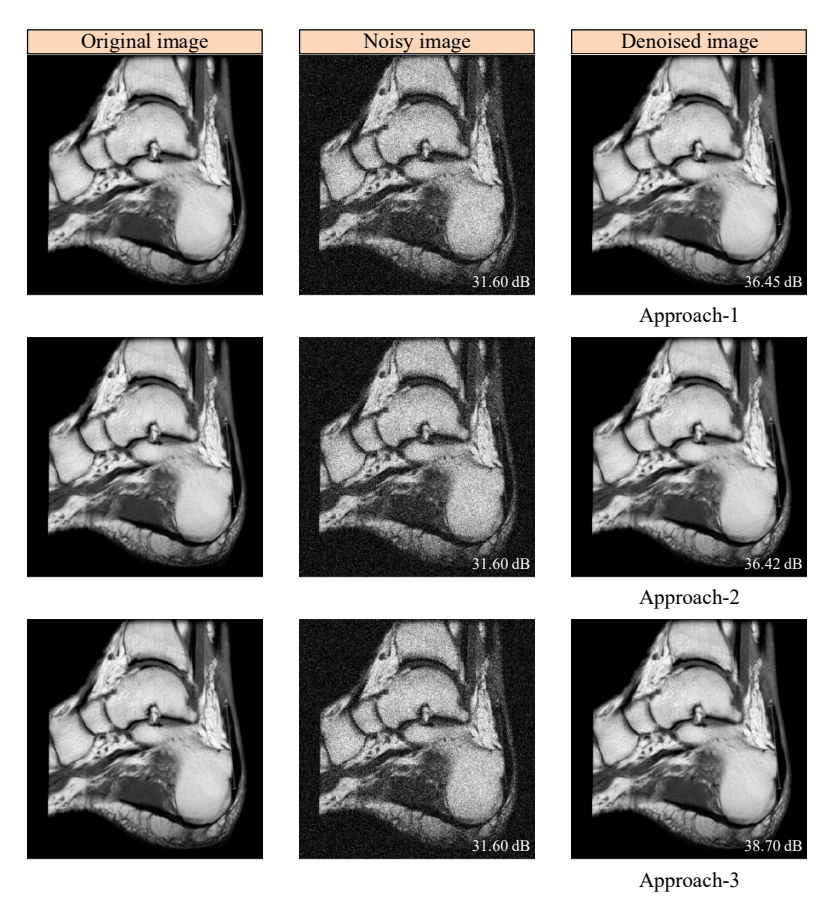


Fig. 7. Sample of denoised MRI images

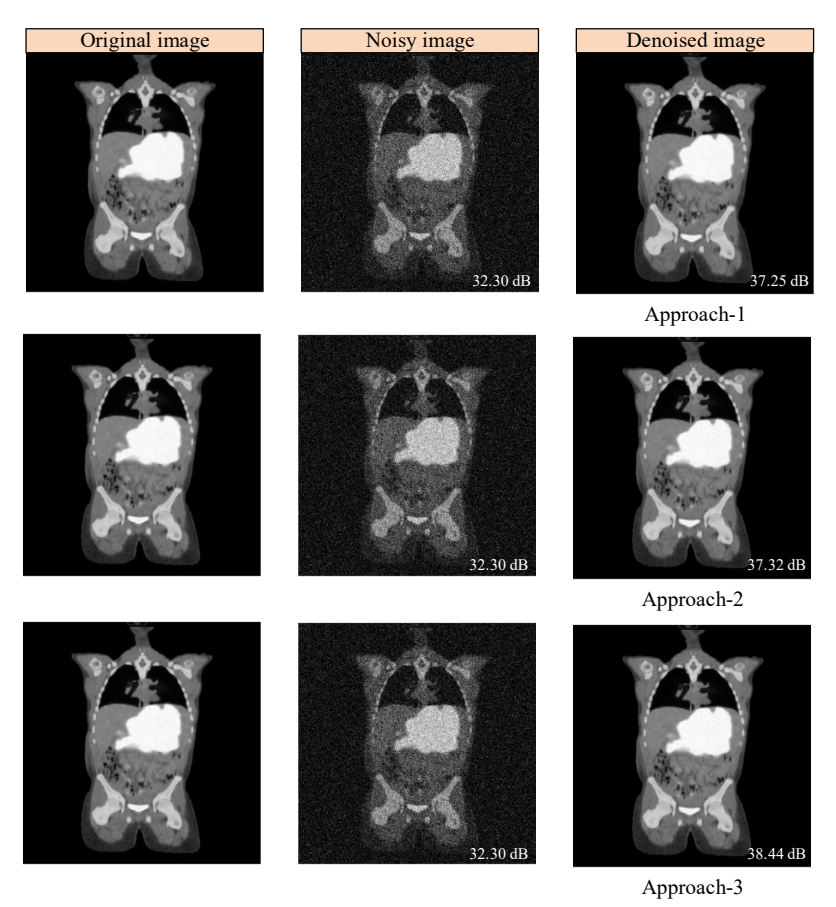


Fig. 8. Sample of denoised PET images

To ensure a fair comparison, the results of the proposed denoising techniques are compared with those from previous studies using the same medical imaging modalities. The performance of CT, MRI, and PET images is evaluated and detailed in Tables 4 to Table 6, referencing studies [26, 27] for CT, [28, 29] for MRI, and [16, 18] for PET. The utilization of various medical image varieties should theoretically result in different results. This is because they are formed by different modalities. This fact has been proven based on the results obtained.

For CT images, Approach-2 produces a denoised image that closely resembles the original, achieving an SSIM value of 0.943. Additionally, Approach-2 delivers a 28 % higher PSNR compared to the results in [27]. Furthermore, it achieves a significant improvement in Gaussian denoising, with approximately 25 % reduction in noise.

In the case of MRI and PET images, Approach-3 outperformed the other approaches by achieving higher PSNR and SSIM values. Specifically, for MRI images, Approach-3 resulted in a significant 26 % increase in PSNR compared to [28], as well as an impressive 18.7 % improvement in Gaussian denoising. For PET images, Approach-3 demonstrated a substantial 25 % rise in PSNR compared to [16] and achieved an approximate 15 % improvement in Gaussian denoising.

**Table 4**Comparison of the denoised performances for CT images

	Method	PSNR (dB)	SSIM		
•	CNN [26]	25.82	0.850		
	FDCvT [27]	30.43	N/A		
	Approach-1	41.20	0.940		
	Approach-2	42.14	0.943		
	Approach-3	41.40	0.942		

**Table 5**Comparison of the denoised performances for MRI images

<u> </u>			
Method	PSNR (dB)	SSIM	
DWT [28]	28.80	0.900	
FDCvT [29]	33.20	N/A	
Approach-1	36.45	0.855	
Approach-2	36.42	0.853	
Approach-3	38.70	0.860	

**Table 6**Comparison of the denoised performances for PET images

0		
Method	PSNR (dB)	SSIM
CNN [16]	28.97	N/A
DWT and FDCvT [18]	36.30	N/A
Approach-1	37.25	0.781
Approach-2	37.32	0.782
Approach-3	38.44	0.784

#### 6. Conclusions

This paper presents the implementation of FDWT and FDCvT algorithms for denoising medical images. The proposed hybrid methods have demonstrated efficient denoising performance, significantly improving PSNR and SSIM values. A comparative study confirms that the combination of FDWT and FDCvT outperforms traditional techniques in terms of image quality.

Ongoing research is focused on implementing region of coding (ROC) extraction to eliminate irrelevant areas in medical images. Additionally, further research is needed to enhance the FDCvT algorithm using various techniques to optimize the efficiency of the proposed denoising methods.

# Acknowledgement

This research was not funded by any grant.

#### References

- [1] Rajalingam, B. and Rainy, P. "Hybrid multimodality medical image fusion technique for feature enhancement in medical diagnosis." *International Journal of Engineering Science Invention (IJESI)*, Page 52-60, (2018)
- [2] P. A. Team, "Diagnostic imaging dataset 2020-21 data." Resreport 1.0, National Health Services (NHS), Nov. (2021)
- [3] Shyamala, N. and Geetha, S. "Fusion model of Modified Wavelet Transform and Neural Network for medical image compression." *International Conference on Electronics and Sustainable Communication Systems (ICESC)*, (2022). <a href="https://doi.org/10.1109/ICESC54411.2022.9885564">https://doi.org/10.1109/ICESC54411.2022.9885564</a>
- [4] Proakis, J. G. and Monalakis D. G. (1996). Digital signal processing principles, algorithms and applications. *Prentice Hall International*, 3rd ed
- [5] Abdelmajid B., Omar B., Mohamed Y., and Abdelhadi R. "Thermal effect analysis of brain tumor on simulated T1-weighted MRI images." *International Conference on Intelligent Systems and Computer Vision (ISCV)*. (2018). https://doi:10.1109/ISACV.2018.8354083
- [6] Farzana S., Kazi L. D. K. and Fardin S. "Improvisation of magnetic resonance imaging (MRI) with development and feasible evaluation of fiber optic sensors: a survey." *International Conference on Advances in Electrical, Electronic and Systems Engineering (ICAEES)*, Page 577-581. (2016). <a href="https://doi:10.1109/ICAEES.2016.7888112">https://doi:10.1109/ICAEES.2016.7888112</a>
- [7] Enzo F. and Nikos P. "Slice-to-volume medical image registration: a survey." *Medical Image Analysis*, (39). Page 101–123. (2017)
- [8] Swati R., Jignesh S. B. and Patra S. K. "An unsupervised deep learning framework for medical image denoising." *Electrical Engineering and Systems Science*, Page 1-22. (2021). https://doi.org/10.48550/arXiv.2103.06575
- [9] Prabhpreet K., Gurvinder S. and Parminder K. "A review of denoising medical images using machine learning." Current Medical Imaging Reviews, 14(5), Page 675–685. (2018). <a href="https://doi.org/10.2174/1573405613666170428154156">https://doi.org/10.2174/1573405613666170428154156</a>
- [11] Aya I., Shuping Z., Federico A., Marcel A. and Shinji K. "Towards ultrasound everywhere: a portable 3D digital backend capable of zone and compound imaging." *IEEE Transactions on Biomedical Circuits and Systems*, 5(12), Page 968 981. (2018). https://doi: 10.1109/TBCAS.2018.2828382
- [12] Utpreksh P., Ranjeet K., Kumar A. and Lee H. N. "Compression of medical image using wavelet based sparsification and coding." *International Conference on Signal Processing and Integrated Networks (SPIN)*. (2017). <a href="https://doi.org/10.1109/SPIN.2017.8049981">https://doi.org/10.1109/SPIN.2017.8049981</a>
- [13] Ketki C. and Jignesh N. S. "Lossless medical image compression using transform domain adaptive prediction for telemedicine." *International Conference on Wireless Communications, Signal Processing and Networking (WiSPNET)*, Page 1026-1031. (2017). https://doi: 10.1109/WiSPNET.2017.8299918
- [14] Satheesh S. and Prasad K. V. S. V. R. "Medical image denoising using adaptive threshold based on contourlet transform." *Advanced Computing: An International Journal*, 2(2), Page 52-58. (2011). https://doi:10.5121/acij.2011.2205
- [15] Jaleel S. J. "Medical image denoising using mixed transforms." *Journal of University of Babylon for Engineering Sciences*, 4(26), Page 272–281. (2018). https://doi.https://doi.org/10.29196/jub.v26i4.804

- [16] Walid E. S., Amira A. M., Anas M. A., El-Sayed M. E. R., Taha E. T., Osama F. Z., Adel S. E. F., Naglaa F. S., Amel A. A. and Fathi E. B. "Deep cnn model for multimodal medical image denoising." *Computers, Materials & Continua*, 73(2):, Page 3795-3814. (2022). <a href="https://doi.org/10.32604/cmc.2022.029134">https://doi.org/10.32604/cmc.2022.029134</a>
- [17] Muhammad A. A., Muhammad A. M., Asif M. and Daxiang C. "Noise removal from medical images using hybrid filters of technique." *Journal of Physics: Conference Series*, Page 1-8. (2020). <a href="https://doi: 10.1088/1742-6596/1518/1/012061">https://doi: 10.1088/1742-6596/1518/1/012061</a>
- [18] Abhishek B., Minakshi B., Punit S. and Mausumi M. "An efficient wavelet and curvelet-based pet image denoising technique." *Medical & Biological Engineering & Computing*, (57), Page 2567–2598. (2019)
- [19] Satheesh S. and Prasad K. "Medical image denoising using adaptive threshold based on contourlet transform." Advanced Computing: An International Journal ( ACIJ ), Vol. 2, No. 2, Page 52–58, (2011). https://doi:10.5121/acij.2011.2205
- [20] Jameel J. S. "Medical image denoising using mixed transforms." *Journal of University of Babylon, Engineering Sciences*, Vol. 26, No. 4, Page 272–281. (2018)
- [21] El-Shafai W., Mahmoud A. A., Ali A. M., El-Rabaie E. S., Taha T. E., Zahran O. F., El-Fishawy A. S., Soliman N. F., Alhussan A. A. and El-Samie F. E. A. "Deep cnn model for multimodal medical image denoising." *Computers, Materials & Continua*, Vol. 73, No. 2, Page 3796 –3814. (2022)
- [22] Aslam M. A., Munir M. A. and Cui D. "Noise removal from medical images using hybrid filters of technique." *Journal of Physics: Conference Series*, Page 1–8. (2020)
- [23] Li Y., Zhang K., Shi W., Miao Y. and Jiang Z. "A novel medical image denoising method based on conditional generative adversarial network." *Computational and Mathematical Methods in Medicine*, Vol. 2021, Page 1–11. (2021)
- [24] Thamilselvan P. "Improving medical image preprocessing using denoising technique." *ICTACT Journal on Image and Video Processing*, Vol. 12, No. 3, Page 2650–2654. (2022)
- [25] Abhishek B., Minakshi B., Punit S. and Mausumi M. "An efficient wavelet and curvelet-based pet image denoising technique." *Medical & Biological Engineering & Computing*, (57), Page 2567–2598. (2019)
- [26] Anandan P., Giridhar A., Iswarya L. and Nishitha P. "Medical image denoising using fast discrete curvelet transform." *International Journal of Emerging Trends in Engineering Research*, 7(8), Page 3760–3765. (2020). <a href="https://doi.org/10.30534/ijeter/2020/139872020">https://doi.org/10.30534/ijeter/2020/139872020</a>
- [27] Prabhishek S., Manoj D., Reena G., Sarvesh K., Alakananda C., Eshan B., Muskan J., Dasharathraj K. S., Jayant S., Harshit D., Nithesh N. and Rahul P. "A method noise-based convolutional neural network technique for ct image denoising." *Electronics 2022*, (11), Page 1–19. (2022). <a href="https://doi.org/10.3390/electronics11213535">https://doi.org/10.3390/electronics11213535</a>
- [28] Lalit M. S. and Pulen D. "Bio-medical image denoising using wavelet transform." *International Journal of Recent Technology and Engineering*, 1(8), Page 2479–2484. (2019)
- [29] Thamilselvan P. "Improving medical image preprocessing using denoising technique." Journal on Image and Video Processing, (12), Page 2650–2654. (2022)